SATELLITE MEASUREMENTS OF ETHYLENE FROM BIOGENIC SURFACE EMISSIONS

A Thesis

Presented to

The Faculty of the Department of Physics and Astronomy

California State University, Los Angeles

In Partial Fulfillment

of the Requirements for the Degree

Master of Science

in

Physics

By

Ninos Y. Hermis

August 2018

The thesis of Ninos Y. Hermis is approved.

Dr. Paul Nerenberg, Committee Chair

Dr. Milan Mijic

Dr. Vivienne Payne

Dr. Radi Jishi, Department Chair

California State University, Los Angeles

August 2018

ABSTRACT

Satellite Measurement of Ethylene (C_2H_4) from Biogenic

Surface Emissions

By

Ninos Hermis

Global chemical model simulations suggest enhancements in near-surface ethylene (C_2H_4) volume mixing ratios (VMR) over tropical land regions from biogenic sources, yet measurements have not been available to test current models. We provide a study to investigate the detection threshold of the trace gas ethylene (C_2H_4) from spacecraft by biogenic sources within the tropical land regions using the Tropospheric Emission Spectrometer (TES), flying on the AURA satellite and the Cross-track Infrared Sounder (CrIS) on-board the Suomi-NPP and Joint Polar Satellite System satellites. Sources of C_2H_4 include petrochemical emissions, fires, and biogenic sources. The typical lifetime of C_2H_4 in the troposphere is 14-32 hours. We sample fields of C_2H_4 VMR from the GEOS-Chem chemistry transport model according to locations of TES and CrIS footprints in order to determine the number of expected measurement points within different areas for different time scales. Over tropical land regions, the model shows profiles of C_2H_4 that peak at the surface, with VMR values of 1.5-4.0 ppbv. An example model profile with elevated C_2H_4 was input to a radiative transfer algorithm to generate a brightness temperature difference spectrum. The magnitude of the C_2H_4 signal was found to be 0.05 K near 950 cm^{-1}. The single-footprint instrument noise was 3 times higher for TES (0.15K) than the signal and equal signal-to-noise for CrIS (0.04K). For single-footprint retrievals of C_2H_4 over tropical land regions to be feasible, signals associated

with elevated C_2H_4 VMR near the surface would need to be higher than the instrument noise. Spatial and temporal averaging of satellite measurements is needed to increase signal-to-noise ratios.

ACKNOWLEDGMENTS

I would like to thank my advisor Dr. Vivienne Payne and my committee member Dr. Paul Nerenberg for their endless patience and guidance on completing this thesis. I would also like to thank other JPL scientists as Dr. Kevin Bowman, TES principle investigator for funding support and the rest of the TES team for all supplemented data. I would also like to thank Dr. Dylan Millet from the University of Minnesota for supplementing his ethylene GEOS-Chem model. I would also like to thank the NASA Jet Propulsion Laboratory for providing me with the tools and opportunity to conduct research and meet with collaborators. This research was supported by the JPL TES project.

Lastly I would like to thank my family and friends for their continued support in my career as a master's student at California State University Los Angeles.

TABLE OF CONTENTS

LIST OF TABLES

Table

LIST OF FIGURES

Figure

CHAPTER 1

Introduction

1.1 Ethylene (C_2H_4) - Role and Reaction in Atmosphere

C_2H_4 is a nonmethane volatile organic compound (NMVOC) or hydrocarbon molecule that is important due to its effects within the Earth's troposphere. Despite its low abundance, C_2H_4 rapidly reacts photochemically with the hydroxyl molecule (OH) which in effect forms carbon monoxide (CO) and lower tropospheric O_3 (Alvarado et al., 2011). The resultant reaction has deleterious health effects which can affect humans and vegetation (Sawada and Totsuka, 1986). The formation of ozone within the troposphere is considered a pollutant vs. ozone in the stratosphere (which protects against UV-radiation) (WHO Study, 2008). Ozone within the troposphere is also considered a greenhouse gas (Lacis et al., 1990; Hauglustaine et al., 1994). Other trace gas reactants include peroxyacetyl nitrate and other carbonyl compounds (Chuong and Stevens, 2000). These reaction with OH molecule does not allow C_2H_4 to remain long in the atmosphere. The mean lifetime of C_2H_4 within the troposphere is approximately14-32 hours (Alvarado et al., 2010), based upon latitude and time of year. Seasonal cycle in northern hemisphere shows highest VMR around February and the lowest in July/August (Blake and Rowland, 1986). The southern hemisphere shows maximum VMR in late winter and minima in summer. Biomass burning in the southern hemisphere also contribute to this seasonal cycle during the months of July/August (Rudolph et al., 1989). Understanding the effects and seasonal cycles of C_2H_4 will help this research in choosing locales and time periods where C_2H_4 measurements would be most sensitive to spaceborne instrumentation.

1.2 Sources of Ethylene (C_2H_4)

C_2H_4 has both anthropogenic and natural (biogenic) sources. It also has emissions due to biomass burning (Sawada and Totsuka, 1986). Estimated emissions are approximately 18-20 Tg/yr (Folberth et al., 2006, Horowitz et al., 2003). Anthropogenic sources come from combustion of fossil fuel waste, refuse incineration, burning of vegetation for the clearing of agriculture and the emissions of ethylene industrial plants. Biogenic sources include plant and microbial activity. Plants use C_2H_4 for a hormone to govern growth and ripening. Excess C_2H_4 can have deleterious effects on the growth of vegetation (Sawada Totsuka, 1986). There are also some biogenic emissions related to the top layer of the ocean near 0.67 Tg/yr (Siefert et al., 1999). The sources of the C_2H_4 emitted from biogenic sources is thought to be comparable to anthropogenic emissions. These emissions can further be broken down to their respective categories. See Table 1. Biogenic sources are the most vital to this research as we are trying to estimate C_2H_4 measurements from spaceborne instruments near the surface.

1.3 Scope of Research

We will demonstrate a feasibility study to identify C_2H_4 volume mixing ratios from a surface biogenic source using spaceborne satellite instrumentation. Chapter 2 provides background on past studies of C_2H_4, as well further information on spectral signature features of C_2H_4 and the limitations to obtaining brightness temperature spectra. Chapter 3 will describe our global dataset selection with its incorporation of global atmospheric model (GEOS-Chem) and inputs for the line-by-line-radiative-transfer model. Chapter 4 will describe the brightness temperature results of the regions chosen

for study and applicability to the TES or CrIS instruments. Chapter 5 will discuss and conclude the results and applicability for future surface C_2H_4 emissions studies.

Table 1

Rates and Sources of C_2H_4 Emissions.

Category	Rate of emissions (Tg/yr)[2]
Biomass Burning	8.63
Fossil Fuel + Industry	4.45
Vegetation	4.30
Ocean	0.67

Note. Estimated global emissions of C_2H_4 from global chemistry transport model with input from various surface and other in-situ measurements over a number of years. Source: Folberth et al., 2006.

CHAPTER 2

Background

2.1 Spectral Signature of C_2H_4

The spectral feature of C_2H_4 is concentrated in the Q branch at 949 cm^{-1}. Figure 1 shows the optical depth feature at the 949 cm^{-1} alongside other trace gases within the spectral range of 940 and 960 cm^{-1} (Dolan et al., 2016). From figure 1 we can compare the optical depth to other various trace gases. We notice the negligible opacity of C_2H_4 versus other trace gases such as HNO_3 or CO_2. The spectra are dominated by H_2O and CO_2, which translates to more opaque molecules.

Optical depth, τ , is the natural logarithm of the ratio of incident and transmitted radiance through a medium.

$$\tau = \ln\left(\frac{\phi_i}{\phi_t}\right)$$

Measuring the optical depth or thickness is done vertically from the top of the Earth's atmosphere to some altitude. This can also be written as:

$$\tau = \int_z^\infty k_{abs}\rho_a dz'$$

Where k_{abs} is the mass absorption coefficient, ρ_a is the medium density through the path length $dz' = ds\ cos\theta$ which is the trigonometric relation for the pathlength through the specified altitude. For the TES instrument a line-by-line-radiative-transfer-model (forward model or LBLRTM) was used to calculate opacity (Clough et al., 2005). From this and using other various inputs for the LBLRTM model (see chapter 3.2), we can generate brightness temperature spectra that shows a specific absorption signal at a specified wavelength for C_2H_4. Other considerations will need to be accounted for, such as

internal instrument noise, which can obscure the absorption signal of the molecule of interest.

Measurements were made via radiance spectra in units of W/cm^2 sr cm^{-1}, which is the flux collected within a solid angle at a specific wavenumber per unit of surface, from the top of the atmosphere. This in turn is then converted to brightness temperature difference spectra (BTD) by inverting the Planck blackbody function (in this case a grey body). The brightness temperature signal will be lower or higher than the unitary emissivity (which is equal to the surface temperature of the Earth = 1), due to absorption and emission processes within the Earth's atmosphere path length. From here, we can determine the absorption and emission features of a particular species by looking at the difference between a perturbed and reference window channel within a spectrum (no C_2H_4). Some sample studies are discussed in the next chapter to show the difficulties in obtaining such measurements.

2.2 Previous Measurements of C_2H_4

Previous measurements of C_2H_4 in the atmosphere has constituted a variety of methods that include surface, airborne, and satellite observations (both limb and nadir). Surface measurements constituted monitoring stations and networks that relayed C_2H_4 concentrations to and from the stations. These included European networks such as the WMO (World Meteorological Organization) program called *Global Atmosphere Watch* (GAW). GAW is a worldwide network of monitoring stations and data centers. There is also the European Monitoring and Evaluation Programme (EMEP) which is designed for monitoring long range air pollution within Europe. Examples of air campaigns to monitor C_2H_4 have come from NASA's TRACE A (Transport and Atmospheric Chemistry near

the Equator Atlantic) experiment which aimed to study high levels of ozone near the equator and over the Atlantic Ocean. ARCTAS (Arctic Research of the composition of the Troposphere from Aircraft and Satellites) was another NASA aircraft campaign aimed to study boreal fire plumes near the Arctic. ARCTAS collected data on gases and aerosols. Past satellite measurements of C_2H_4 were contained to specific fire plumes, roughly averaging 3-6 km in height (Dolan et al., 2016). These plumes would be lofted to the troposphere, along with their constituent trace gases. Various orbiting satellites carry onboard limb or nadir Fourier spectrometers (see table 2) that attempted to measure C_2H_4. Both varieties of surface and satellite observations were sometimes used together to measure C_2H_4 in the atmosphere.

2.2.1 Different Types of Satellite Measurements (Limb vs. Nadir)

A study using a limb geometry, conducted by Herbin et al (2009), showed distributions of C_2H_4 in the upper troposphere using the Canadian limb sounder ACE-FTS instrument. ACE-FTS instrument onboard the SCISAT satellite, is a Fourier transform spectrometer within the range of 750 to 4400 cm^{-1} with a spectral resolution of 0.02 cm^{-1} (Herbin et al. 2009). This instrument operates in solar occultation mode, waiting for sunrises and sunsets to measure transmittance spectra containing volume mixing ratios of gases and aerosols, hence a limb sounding instrument. Vertical profiles were obtained from 5-20 km from infrared solar occultation spectra in 2005 and 2006. These were measured in remote Arctic regions at high latitudes. The spectral window was 949.86 – 950.88 cm^{-1}. Background volume mixing ratios, temperatures, and pressures were measured over a two-year period. The signal for C_2H_4 is represented in the transmittance spectra in figure 4. From a limb viewing geometry, spectra are taken through a portion of

the atmosphere where the sun is in the background. As light from the sun passes through the atmosphere, photons are scattered or absorbed by various molecules. We then calculate an absorption spectrum to see where C_2H_4 signal is strongest. Such a signal is prevalent at around 92 pptv. This coincides with elevated levels of C_2H_4 in northern latitude regions (Herbin et al., 2009). For ACE-FTS, the threshold of detection is around the 20 pptv for all altitudes within the troposphere (Herbin et al., 2009). Other lower values retrieved in this study have significant error greater than 100%. Higher VMR values are normally detected from specific lofting processes, such as fire plumes, or outflow of continental pollution. Lower VMR concentration, usually higher in troposphere, is due to more vertical and horizontal mixing, and also due to short mean lifetimes of C_2H_4 as it chemically interacts with free radicals. The study was also hindered in collecting concentration VMRs from either the ocean or near surface, due to non-lofting processes. Latitudinal measurements helped to retrieve better signal-to-noise measurements, especially near the poles, where the measurements occurred.

This study exhibits the limitations of limb-viewing geometry. From the Herbin et al study we see results for C_2H_4 detection at high altitudes only. This detection threshold is much lower (more sensitive) than the nadir detection threshold. The limb measurements in Herbin et al. paper show variations of ~10-20 parts per trillion. Lofting processes are required over a period time to ascertain a reliable molecule detection, particularly within the troposphere. There were also limitations to retrieving ocean or near surface detections, because there were very few lofting processes over the ocean. The physics of the limb-viewing has significantly longer path lengths or optical depths to

traverse through, versus the shorter pathlength geometry of nadir (top-down) viewing. Our next study will show the advantages to nadir viewing geometry.

One study showing the nadir geometry viewing was the Coheur et al. (2009) study. The study showed measurements using the European Infrared Atmospheric Sounding Interferometer (IASI). IASI, launched in 2006, is a cross-track scanner onboard the Metop-A polar orbiter platform. Spectral coverage is from 645 to 2760 cm^{-1}, with a spectral resolution of 0.5 cm^{-1} (Clarisse et al., 2011). Coheur et al. showed a distinct signature in the IASI infrared spectra for C_2H_4 among other trace gases in an atmospheric window 800 to 1200 cm^{-1} from particularly strong fires that occurred in the Mediterranean Basin in August of 2007 and the eastern Siberia region in 2008. The study showed results of several trace gas species as peroxyacetyl nitrate (PAN), ammonia, ethylene, methanol, and formic acid. The Coheur et al study showed residual spectra from the plume (figure 2). These were calculated by taking reference spectra nearby without fires (grey lines) and one from the plume. The residual spectrum is indicated in red which shows features relating to a particular species. In calculating the BTD, we can observe the limitations of such spectra and the sensitivity needed to be able to detect multiple species either from the surface or from a plume. These detection limits are due to vertical sensitivity and the unknown plume height. Also, the species involved may have short lifetimes due to chemical interactions within the troposphere and dilution within the ambient air. Figure 3 shows a column density map for a Greece fire plume. From the figure we can see the enhanced concentration of molecules per mol/cm^2 in the plume versus the background (in green and blue). The total columns observed for all fire plume species come with statistical errors between 5-30% (1σ) (Coheuer et al., 2009).

The third and last study mentioned in this paper, is another nadir study by Alvarado et al. (2011) using the Tropospheric Emission Spectrometer (TES) onboard the AURA satellite. Their research was conducted in conjunction with the ARCTAS-B campaign. They used TES retrievals to calculate the C_2H_4 VMR in contrast to CO within the fire plumes. From these retrievals they were able to detect VMR of C_2H_4 to approximately 2 ppbv in fresh fire plumes. These measurements agreed with the aircraft campaign measurements and other various surface measurements. For example, plumes were identified by corresponding CO concentrations from various biomass burning regions from the Atmosphere Infrared Sounder (AIRS) to the TES retrievals. A plume was identified by TES observations as an area with a volume mixing ratio to be 150 ppbv (Alvarado et al., 2011) at 510 hPa pressure level. From these plumes, brightness temperature difference spectra were created in reference to a specific profile retrieval, calculated and compared to a priori data from the GEOS-Chem model. This spectrum depends on the limits of the strength and location of peak C_2H_4 mixing ratios and the thermal contrast of the atmosphere at the given time of the scan. Such scans also include factors of cloud optical depth, emissivity, reflectivity, and temperature (see chapter 3.2). The model is included in the above-mentioned parameters in TES data files. From this study we conclude that surface emissions of ethylene are possible from the 1-2 ppbv range. But this strongly depends on the limiting detection factors as that expressed by the C_2H_4 retrievals such as location of plume, thermal atmosphere factors, and TES S/N factor.

2.2.2 Dolan et al. (2016) Study

A study that analyzed some of these limiting factors was Dolan et al. (2016). This was a follow-up study from measured boreal fire plume observations by Alvarado et al.

(2010) using the step-and stare method via the TES instrument. The TES observations were used in support of the ARCTAS summer phase of its mission in 2008 (Dolan et al., 2016). Dolan et al. used these observations to detect C_2H_4 within the plumes and tested to see if it would be feasible to detect VMR near the surface. An initial optical depth plot of C_2H_4 was created as a model to define the strength C_2H_4 signal. An LBLRTM (Clough et al., 2005) model was used with parameters input from the High-Resolution TRANsmission molecular absorption (HITRAN) database (Rothman et al., 2003) at 949 cm^{-1} (Figure 1) alongside other trace gases. The spectra showed its optical depth in contrast to the other trace gases. In this case the C_2H_4 optical depth was much smaller than that of other trace gases. All other parameters, such as atmosphere temperature, surface temperature, and surface emissivity are all routinely retrieved via the TES instrument and input in LBLRTM. BTD plots were created to show spectral feature at 949.3-949.5 cm^{-1} minus all other background features.

The detection limit needed to be assessed from the TES brightness temperature spectra, which is based on the plume height (z_0) and width (σ). An LBLRTM model was run with background concentrations of 0.04 ppbv with varying z_0 and σ to determine the maximum VMR above the 0.15K instrument noise. The model also calculated plots which show high detection limits when C_2H_4 peaks near the surface, with a high thermal contrast. Thermal IR radiances are more sensitive to VMR's in the free troposphere rather close to the surface (Figure 7). Also, when the plume height increased, the detection threshold decreases in ppbv. Near surface detection may be possible at the 2-3 ppbv with spatial averaging of spectra, which are non-fire plume sources.

Table 2

Breakdown of major atmospheric satellites with ranges and resolutions capabilities

Satellite	Spectral Range	Resolution	Launch Date
ACE-FTS	750 - 4400 cm^{-1}	0.02 cm^{-1}	2003
TES	650 - 3050 cm^{-1}	0.06 cm^{-1}	2004
IASI (MetOp-A)	645 - 2760 cm^{-1}	0.5 cm^{-1}	2006
CrIS (SUOMI)	650 - 2550 cm^{-1}	0.625 cm^{-1}	2011

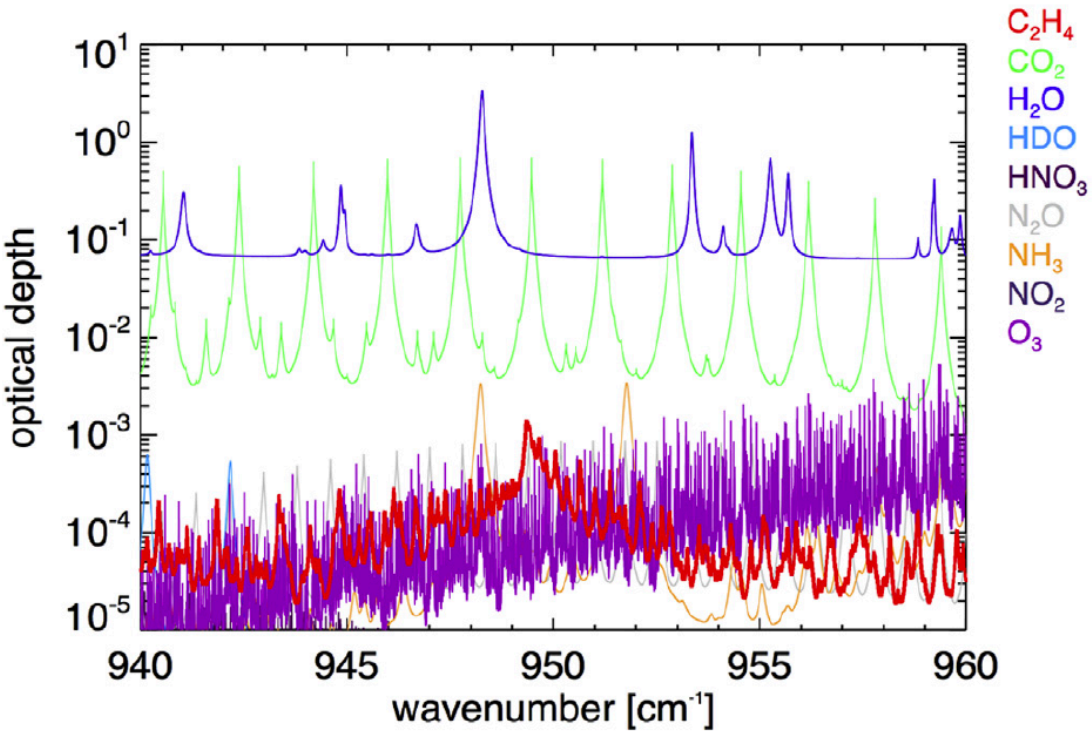

Figure 1. Optical depth features with the C_2H_4 feature at 949 cm^{-1}. The strongest absorption features represented are from H_2O and CO_2. Other various trace gases are also seen from wavelength range of 940 to 960 cm^{-1}. Source: Dolan et al., 2016

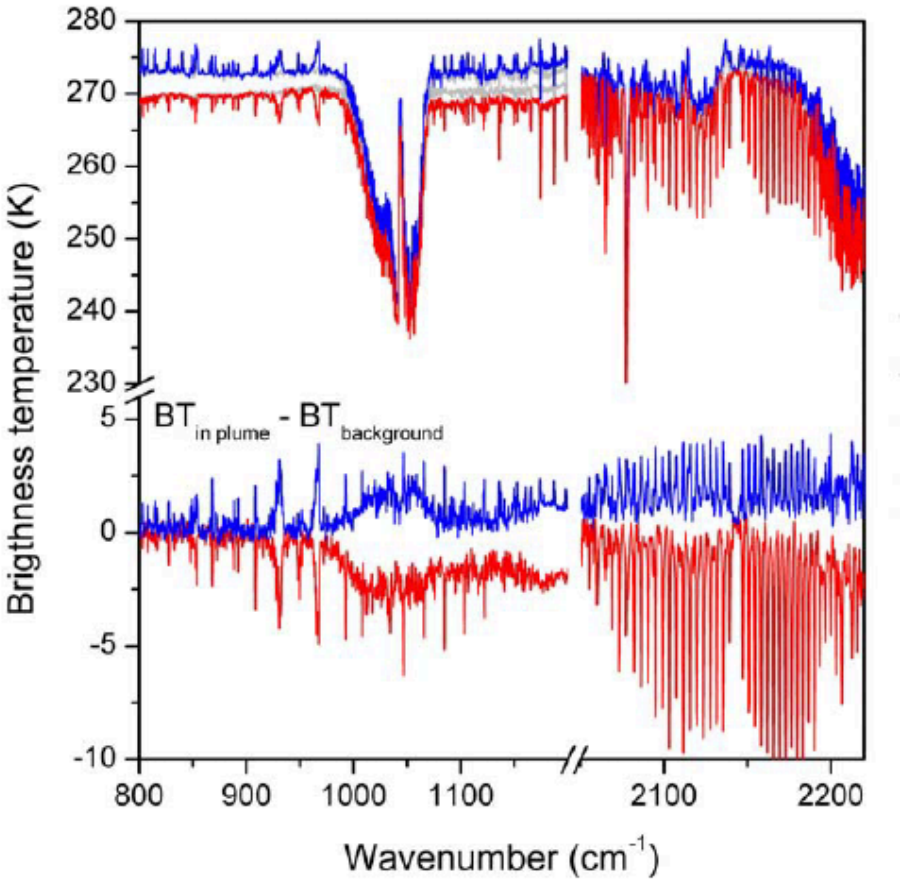

Figure 2. Brightness temperature difference spectra (BTD) of ammonia from fire plumes in Baikal Siberia 2008. The spectra are shown, one with the background spectra (above) and the second (below) showing the residual. The residual is obtained by subtracting the nearby background spectra (grey line). The positive blue lines are emissions and red negative line are absorption of features within the fire plume. Beyond the 2100 cm^{-1} is the CO signature compared to the background concentrations. CO is clearly a residual trace gas emitted from such fire plumes. We will examine this result in this study.
Source: Coheur et al. 2009.

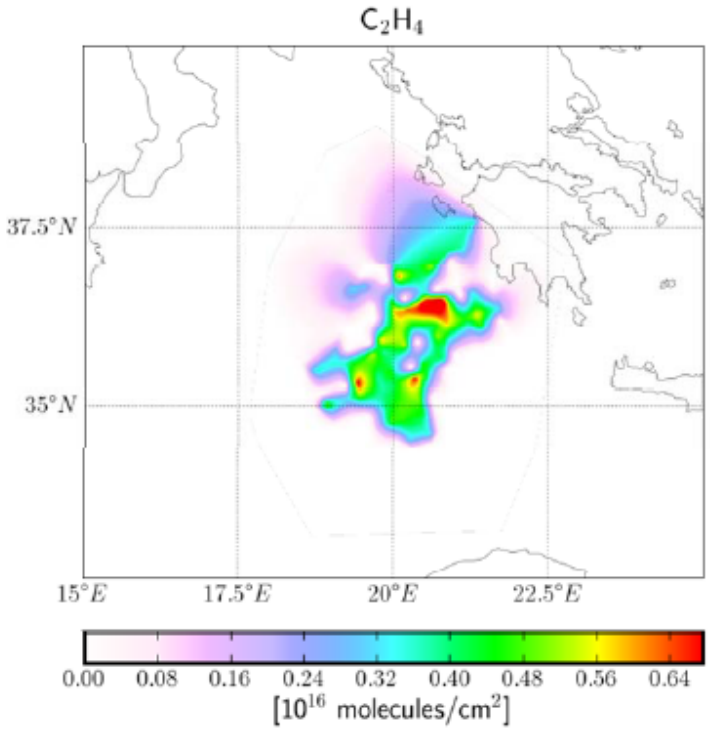

Figure 3. Fire plume from the Peloponnese fires, column density map showing C_2H_4. Source: Coheur et al., 2009.

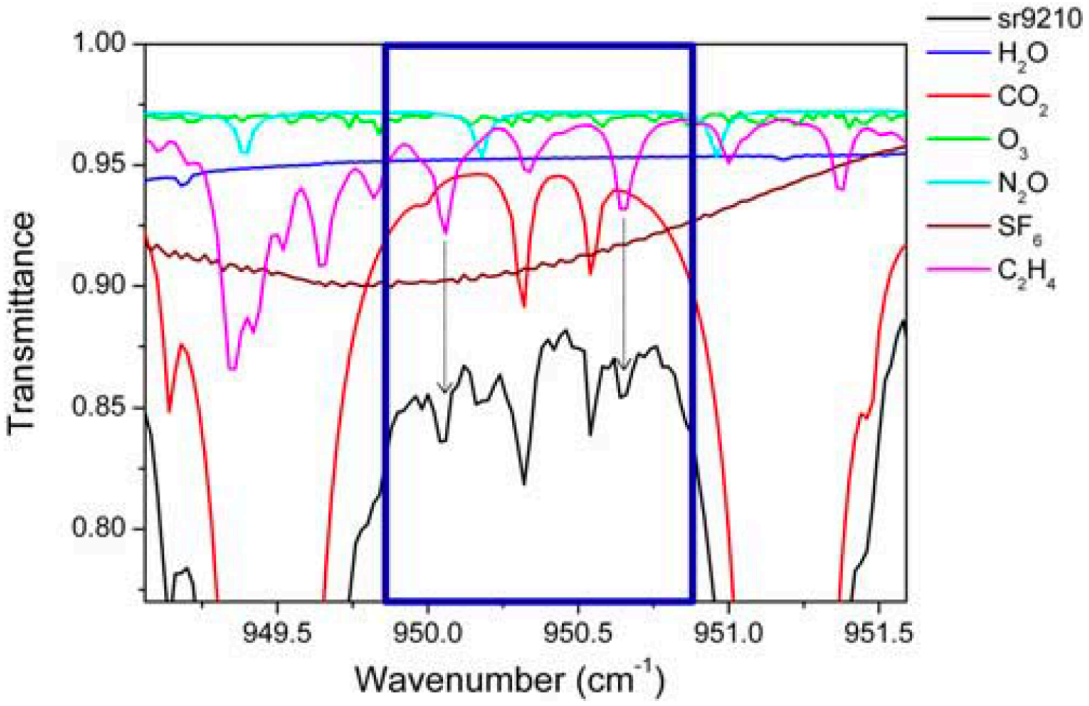

Figure 4. Ethylene spectral signature seen roughly around 950 cm^{-1} and 950.5 cm^{-1}. The black line shows actual measured spectrum from ACE-FTS, while the colored lines show simulated spectrum molecule-by-molecule. Source: Herbin et al., 2009.

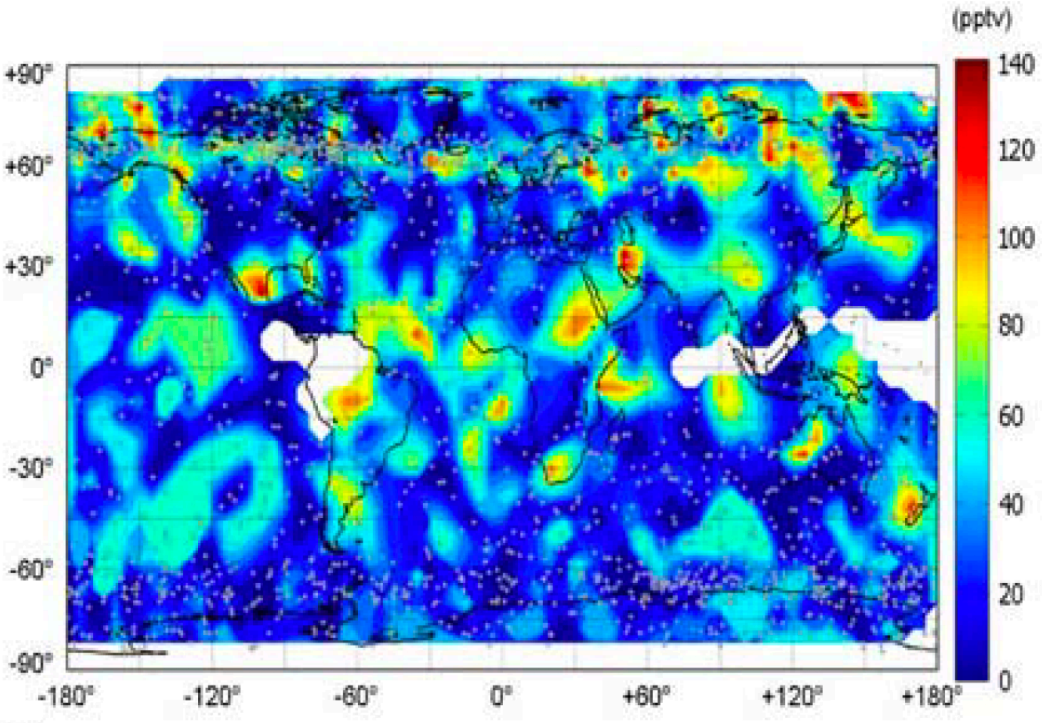

Figure 5. Volume mixing ratios of ethylene in pptv. The blue areas indicate VMRs well below 100 pptv, while the yellow and red colors indicate concentrated C_2H_4 VMRs usually due to continental pollution and other lofting processes. Source: Herbin et al., 2009.

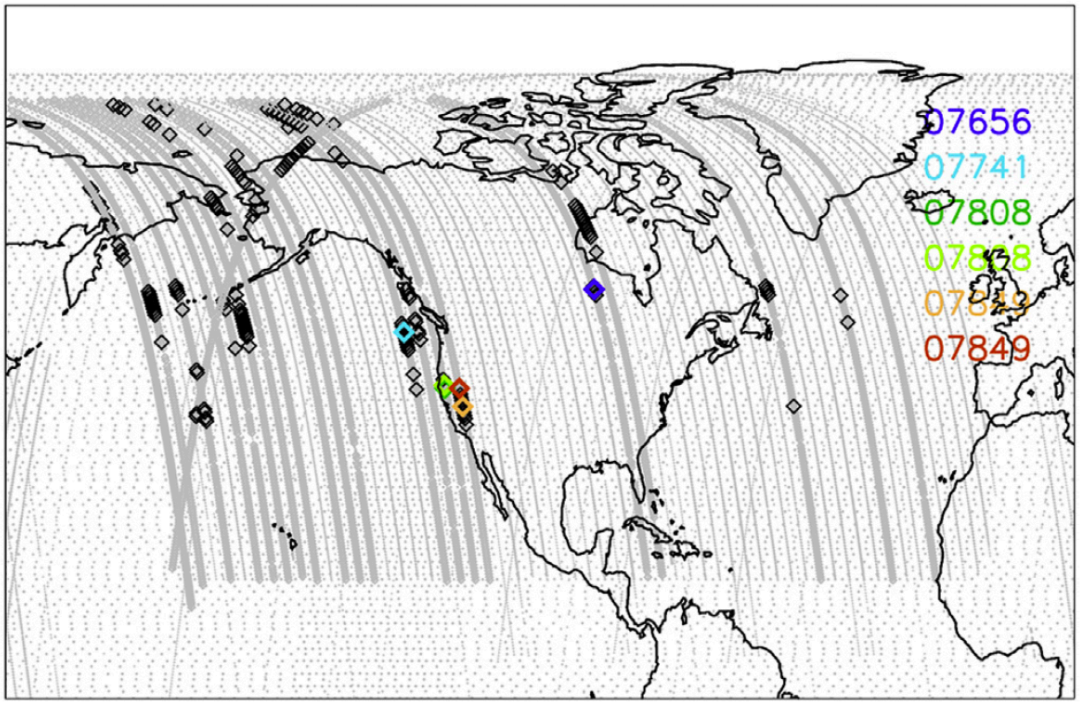

Figure 6. TES observations of boreal fire plumes in 2008(small grey points). The tracks show TES footprints. Black points correspond to CO detection in the 500-mbar pressure with VMRs of >150 ppbv. Colored points are location of fire plumes discussed in Dolan et al. (2016) with confidence of detection of C_2H_4 in residual spectra at S/N greater than 2σ. Source: Dolan et al., 2016

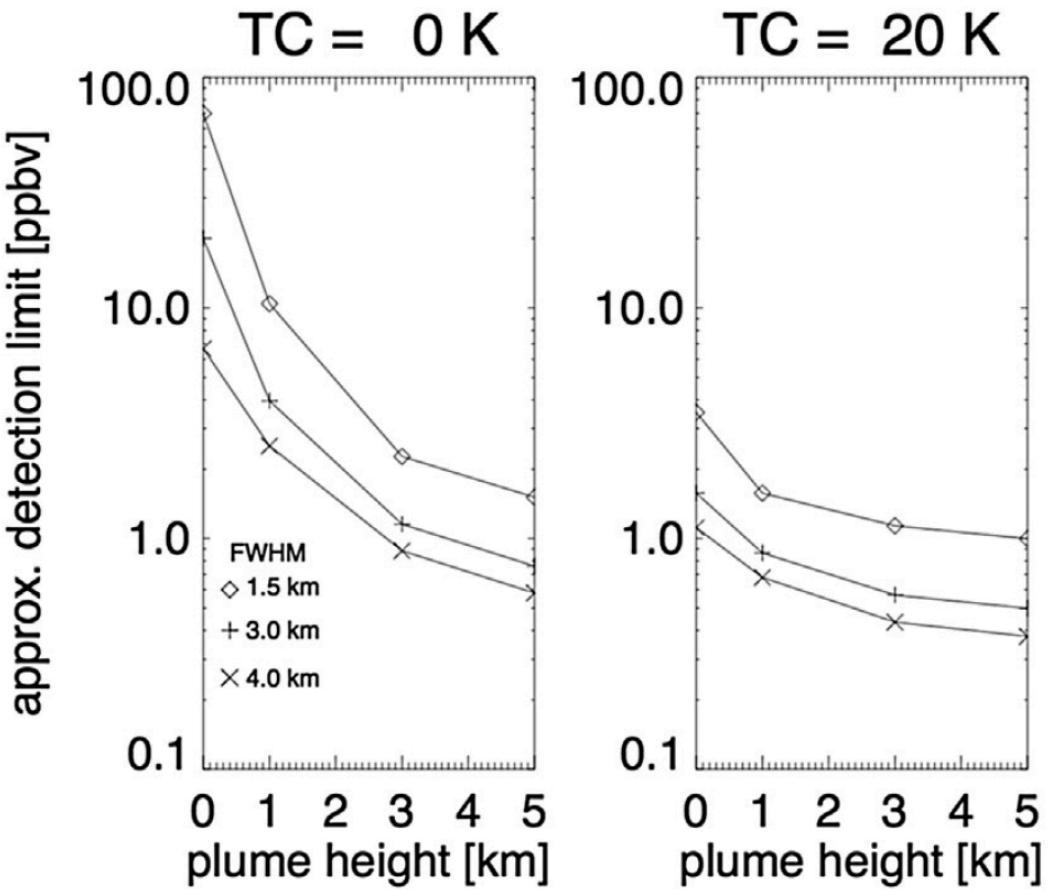

Figure 7. VMR sensitivity detection dependent on thermal contrast from surface to top of atmosphere or the altitude of lofted C_2H_4. Zero thermal contrast from surface to some altitude of lofted C_2H_4 needs more significantly more VMR for detection, while higher thermal contrast of 20 K, lowers VMR detection threshold VMR. Source: Dolan et al., 2016

CHAPTER 3

Data Sample Selection and Models

3.1 Satellite Characteristics

The two instruments we have chosen to model the surface detection of ethylene are the Tropospheric Emission Spectrometer onboard the Aura satellite (Beer et al., 2001) and the NASA Cross Track Infrared Sounder (CrIS) onboard the JPSS or SUOMI satellite. I will compare and contrast the two datasets from both satellites and further explain why we chose specific timeframes as opposed to others. I will also show specific spatial sampling of both instruments, along with their spectral resolutions and noise characteristics. The latter will be extremely vital in helping us to test satellite sensitivity for surface C_2H_4 detections.

TES is a nadir instrument on board the Aura satellite, which has been in orbit since 2004 and was recently decommissioned in January 2018. TES is a Fourier transform infrared spectrometer with a spectral range in the thermal IR from 650 to 3050 cm^{-1} and a spatial coverage (footprint) 5.3 x 8.5 km nadir (16 detectors, 0.5 km by 5 km for each). TES is a 16-element detector array (Beer et al. 2001). TES utilizes a variety of observation modes including the step-and-stare mode and transect. In this study we use the global survey mode (Beer et al. 2001), which collects data every 40km along the TES flight path for a specified number degree latitude. This mode has a high spectral resolution of 0.06 cm^{-1} (0.1 cm^{-1} apodised). Data measured include atmospheric temperature, surface emissivity, cloud height, and cloud optical depth (Kulawik et al., 2006). The TES global survey data we used was for the year 2009. The instrument was operating well and providing good coverage in 2009. In years after 2009, instrument

aging issues led the TES team to change the observing strategy, resulting in a reduction in spatial coverage. Retrieval products include a variety of gases as PAN, O_3, H_2O, CH_4, NH_3, and CO.

The CrIS instrument onboard the Suomi NPP (2000) or JPSS (2017) satellites provides more accurate meteorological data such as atmospheric temperature, moisture, and climate. CrIS has a sun-synchronous orbit, with a spectral range of 650-2550 cm^{-1} and a spectral resolution of 0.625 cm^{-1}. CrIS is across-track scanning instrument with a 2200 km swath width. While the spectral resolution is not as high as TES, it has a much larger spatial coverage. CrIS also has a spectral noise of ~0.04K in the spectral range of interest, while TES is ~0.15K also within the spectral range of interest. Instrument noise will be a determining factor in processing a high S/N for C_2H_4 detection.

3.2 Forward Model Simulations

The TES and CrIS instruments' retrieval of trace gas profiles currently uses radiance spectra in conjunction with radiative transfer calculations by a line-by-line-radiative-transfer-model (LBLRTM) or more generally the forward model. In order for TES and CrIS to retrieve optimal radiances for tropospheric constituents, a robust and fast forward model is needed. The forward model calculates the spectral radiances from the raw measured radiances by the TES and CrIS spectral radiometer. The forward model will need other inputs to characterize the radiating atmosphere and the surface (Clough et al., 2006). The model also contains the instrument internal biases and characteristics to adjust for more accurate radiance measurements.

The forward model or LBLRTM has a specific set of key inputs and outputs, which I will describe here. First, the forward model needs atmospheric pressure levels

and spectral grids in order to perform the calculations necessary. This is supplied by nadir measurements. This contains 87 pressure levels in hecta Pascal (hPa) (Clough et al., 2006). Surface pressures (both sea and land) are determined by available meteorological data. Next, a spectral grid is necessary (per specific TES and CrIS spectral filter) at the top of Earth's atmosphere. Each grid is separated within a specific wavelength. Absorption coefficients are needed to compute radiances for each spectral grid (usually from HITRAN database). These are predetermined and stored within an operational forward model. In the LBLRTM there is a line-by-line calculation of molecular absorption. The next source of input is to calculate the layer pressures and temperatures throughout the path length of the entire Earth's atmosphere. This is performed doing ray tracing and calculating path integrals (Clough et al., 2006). Other inputs are surface altitude, z_0, the instrument viewing angle and averaged emissivity. From the first item on the input list, we will need the model profile of C_2H_4 within the Earth's atmosphere. This was taken from a global atmospheric chemistry transport model.

3.3 GEOS-Chem Model and Vertical Distribution of C_2H_4

A model developed to incorporate a model profile for C_2H_4 is the (GEOS) chemistry transport model (GEOS-Chem). This is a global three-dimensional model of tropospheric chemistry (Bey et al., 2001). The "GEOS" is the transport for a global system. The GEOS model is maintained at Goddard. The GEOS-Chem model uses GEOS meteorological fields (for transport) together with a chemical model. It consists of a total of five models used in the GEOS-Chem system: Atmospheric General Circulation Model, Ocean General Circulation Model, Atmosphere-Ocean General Circulation model, The Chemistry-Climate Model, and the Chemistry Transport Model. All five components use

multi-satellite data for meteorological purposes (https://gmao.gsfc.nasa.gov/GEOS_systems/). The GEOS-Chem model was developed at Harvard University.

In this study we are using this model to predict C_2H_4 vertical distribution (as volume mixing ratios) to incorporate into our LBLRTM model to generate brightness temperature difference spectra. Our collaborator at the University of Minnesota, Prof. Dylan B. Millet, used the GEOS-Chem model to provide monthly, global three-dimensional fields of C_2H_4 VMR's. We sampled the GEOS-Chem model at specific TES and CrIS radiance measurements locations (latitude and longitude) and simulated atmospheric profiles of C_2H_4 from the Amazon, Sub-Saharan Africa, and south-east Asian regions (see Figure 8). From these profiles we are able to estimate that C_2H_4 has the largest VMR from 1000 to around 700 mbars (or hPa) (for pressure levels we restricted to). This would be the ideal range to target for biogenic surface VMR for C_2H_4 along with choosing the right locales for large emissions of C_2H_4.

The GEOS-Chem model was sampled temporally and spatially for TES and CrIS footprints. We extracted TES footprints for the duration of the entire year of 2009 and 2013 for CrIS. We generated monthly global maps indicating the highest estimated VMR's of C_2H_4 within those time frames. The highest global VMR's came from three geographic locations and three different months (see Figures 9, 11, and 12). The figures show three months of the highest elevated levels of near surface C_2H_4 within three different geographic locations. We restricted our sampling to a profile of greater than 700 mbars. The maps show the average VMR for pressures near the surface in areas where there is elevated C_2H_4 VMR. We show an *average surface* VMR in the lower

atmosphere rather than just surface VMR, because we do not expect the thermal infrared satellite measurements to be sensitive at the surface (see chapter 2.1.2). Surface emissions can come from industrial pollutants, seasonal forest decay/growth and biomass burnings. As we have seen from the previous studies (Dolan et al., 2016, Coheur et al., 2009), fire plumes also coincide with elevated CO emissions. We can attempt to show where there are global fires, there will be elevated C_2H_4 molecules. We can conversely show that elevated C_2H_4 VMR does not have to coincide with fire plumes or fire sources rather biogenic sources (Figure 10). These would be prime temporal and spatial areas for spaceborne satellites to target.

3.4 MOPPIT Satellite Data for CO

To further supplement our view of biogenic sources we can compare elevated C_2H_4 VMR global maps to global carbon monoxide (CO) maps. CO is emitted largely through natural processes as photochemical, volcanic and biomass burnings or other combustive processes. Here we generate CO maps via the MOPITT (Measurement of Pollutants in the Troposphere) instrument (Drummond JR and Mand GS, 1996). The Canadian instrument was launched in 1999 onboard the Terra satellite via NASA. MOPITT's main purpose is to understand the distribution, transport and source of carbon monoxide emissions. MOPITT measures in infrared radiation from 4.7μm and 2.4μm. It is a nadir satellite, with a spatial resolution of 22 km. It observes in swaths of 640 km wide and can measure CO in 5 km levels through vertical columns of the atmosphere (Drummond JR and Mand GS, 1996). We generated global maps for the same time periods to further underscore the simultaneous emissions of CO and C_2H_4 and also show that periods of elevated C_2H_4 VMR do not correspond to elevated levels of CO which may

confirm biogenic surface emissions (see figures 9,10,11, and 12). The highest concentrations of C_2H_4 indicate 4 ppbv with MOPITT showing similar abundance in different units of column density (mol/cm). The three regions and various time periods indicate possible different sources of C_2H_4.

3.5 Varying sources of C_2H_4

The South American Amazon region (-70° and -55° lon and -28° and 4°lat) indicates C_2H_4 levels at 4 ppbv in the month of September. During this time, the Amazon undergoes one of its driest periods, with minimal rainfall (Li et al., 2006). The dry period could indicate ripening and drying of vegetation, with an emission of C_2H_4 from the surface. Forest fires are also possible during the dry period, whether natural or anthropogenic in nature. Being in the Amazon limits an anthropogenic cause due to a limited industrial area. More frequent data from the same time period might suggest more natural sources of C_2H_4 emissions.

Surface atmospheric gases have attributed in deriving both northern and southern hemisphere season cycle sources of C_2H_4 and other trace gases (Rudolph et al.,1989). Austral winters (July-Oct) produce C_2H_4 maxima, while austral summers (Dec-Feb) produce C_2H_4 minima (Rudolph et al., 1989). The periods of maxima C_2H_4 emissions have an anthropogenic source as well, which may contribute to the seasonal cycle (Rudolph et al., 1989). The southern hemisphere NMVOC's are likely attributed to biomass burning and emissions from plants (Rudolph et al.,1989). Other anthropogenic sources may contribute much less as they do in the northern hemisphere (Rudolph et al., 1989). Ethylene's photochemical lifetime sustains for longer periods in the summer months versus the winter months in the southern hemisphere (Rudolph et al., 1989). This

considers the reaction with O_3 and OH radical, as there is more abundant NMVOC's in the summer months, hence longer reaction rates occur.

The South Asian region at 92° to 112° longitude and 16° to 30° latitude, also exhibits similar elevated levels of C_2H_4 and CO in the month of September for 2009. Since these areas are mostly industrial, such emissions can likely be attributed to industrial toxic pollutants, once again indicating possible fire plume sources (Rudolph et al., 1989). Other sources can also be attributed to forest photochemical effects, such as dying or ripening of vegetation. This specific locale, neighboring Burma and Thailand, contains some of the worlds densest forest coverage, implying either massive decay or growth of vegetation leading to biogenic C_2H_4emissions. Yet, China's effect of industrial emissions can also contribute to a significant increase in NMVOC's within the region.

We show that different regions contribute varying sources of C_2H_4. We can narrow the source by co-locating CO for possible burning sources, yet we can also exclude high CO sites and see where high C_2H_4 sources occur, which constrict the source emitter to a more biogenic nature. This would be our satellite target to measure C_2H_4 VMR and quantify a known pollutant not just from anthropogenic causes but nature itself.

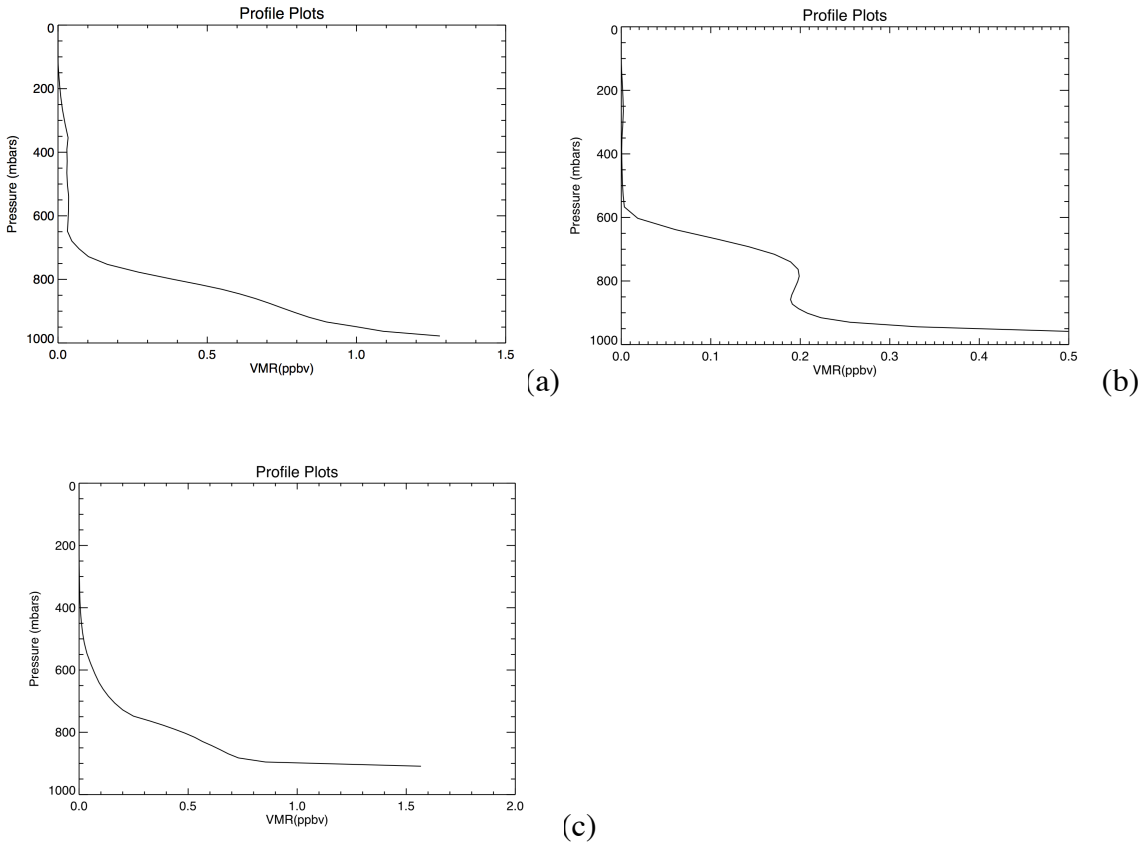

Figure 8. (a) Model profile from the GEOS-Chem chemistry transport model simulating average C_2H_4 VMR sampled at specific CrIS measurement locations, showing the largest concentration VMR located near the surface (pressures greater than 700 mbar) from within Amazon region (-70° to -55° longitude and -28° to -4° latitude). Average VMR count increases as we near towards the surface. (b) Model profile of C_2H_4 VMR over Sub-Saharan Africa (0° and 45° longitude and 0° to 14° latitude). Plot does not show smooth flux of emitting C_2H_4 VMR, yet, around the 700 mbar region could indicate a lofting process possibly from biomass burning. This would not constitute as a surface emission. (c) Model profile of C_2H_4 VMR over Asian region (92° to 112° longitude and 16° to 30° latitude) showing relatively smooth flux of C_2H_4 VMR indicating a possible biogenic source.

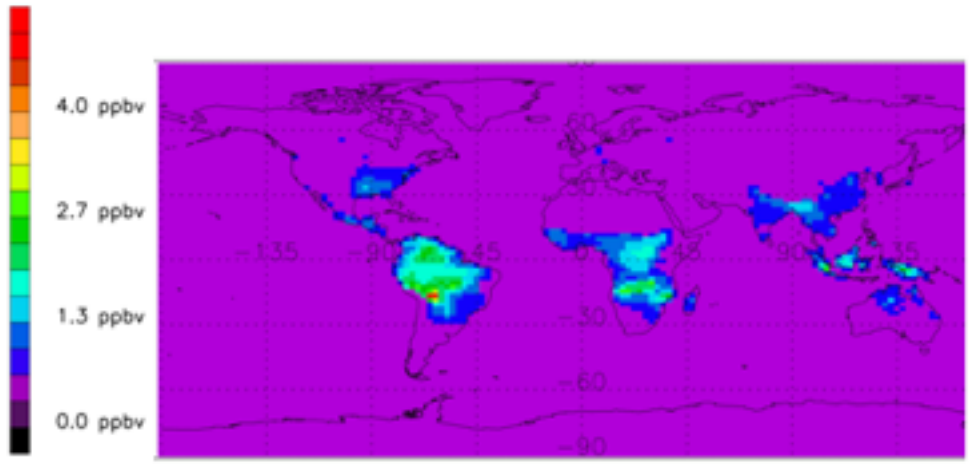

(a)

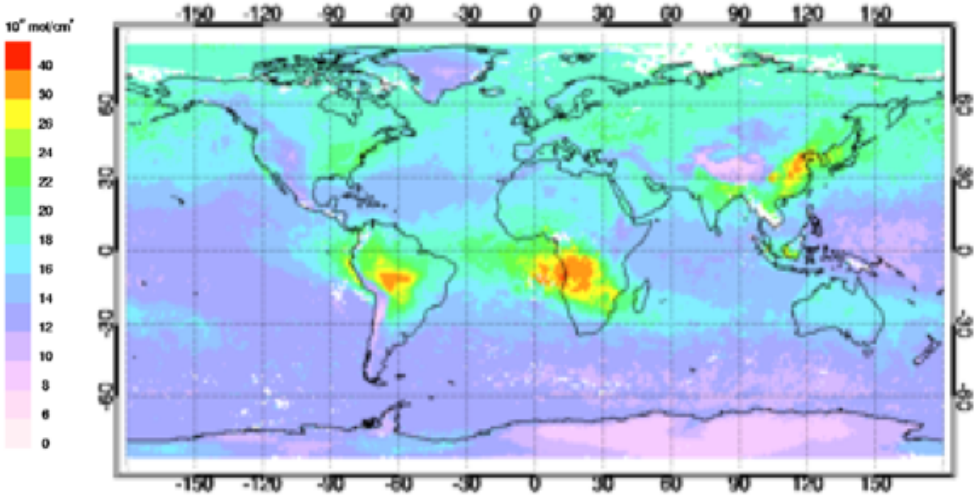

(b)

Figure 9. (a) GEOS-Chem model estimated highest global average emissions of C_2H_4 primarily in the Amazon regions in South America (-70˚and -55° lon and -28° and 4°lat) in the month of September 2009. This indicates all volume mixing ratios greater than 700 mbar, the highest being over 4.0 ppbv. (b) MOPPITT map showing highest elevated levels of CO in 2013 for month of September, indicating a co-location between the same time periods of global CO and C_2H_4 emissions.
(Source: https://www.acom.ucar.edu/mopitt/MOPITT/data/plots/maps.html)

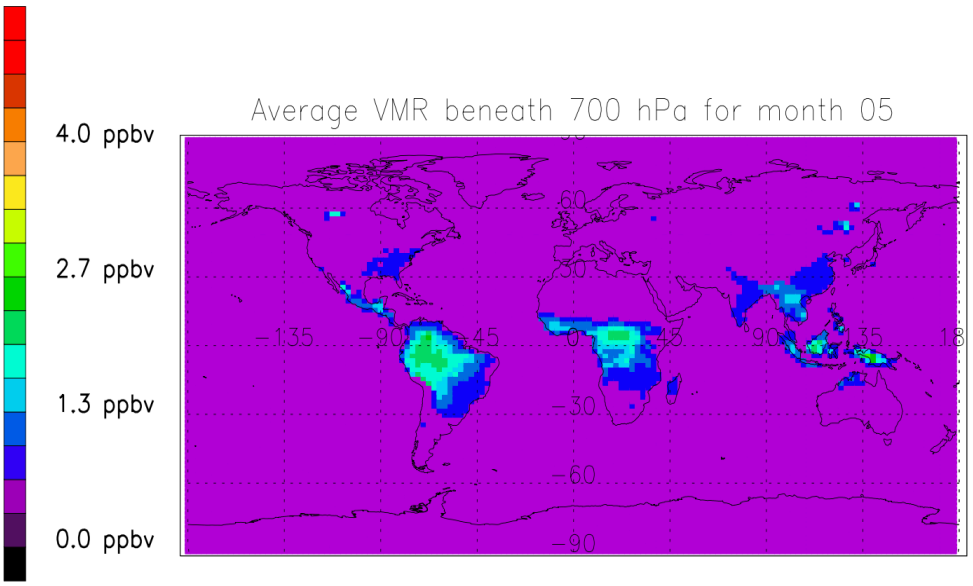

(a)

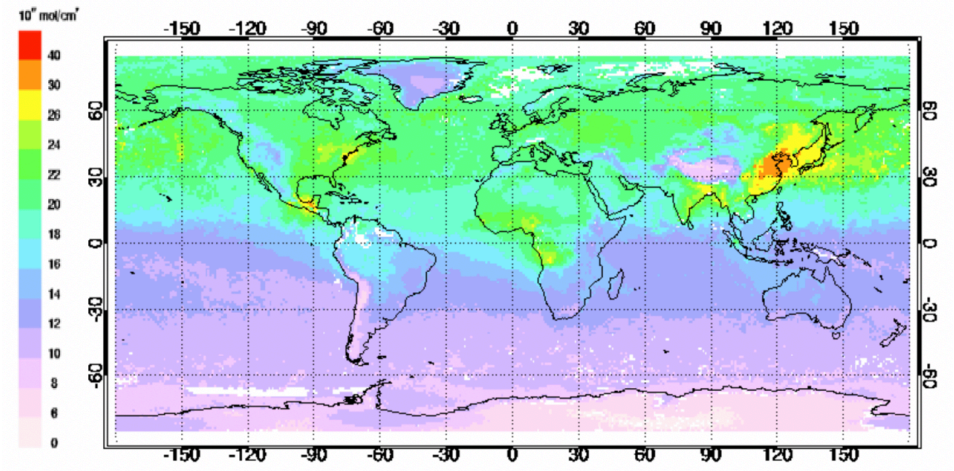

(b)

Figure. 10 (a) Possible biogenic surface C_2H_4 VMR's from GEOS-Chem model primarily in the Amazon regions in South America region (-70˚and -55° lon and -28° and 4°lat) in the month of May 2009. This indicates all volume mixing ratios greater than 700 mbar, the highest being over 2.7 ppbv, indicates a relatively high C_2H_4 period. (b) MOPPITT map showing lowest elevated levels of CO in 2013 for month of May, indicating possible non-fire plume (biogenic) source for C_2H_4 for similar time period of relatively high C_2H_4 emissions.
(Source: https://www.acom.ucar.edu/mopitt/MOPITT/data/plots/maps.html)

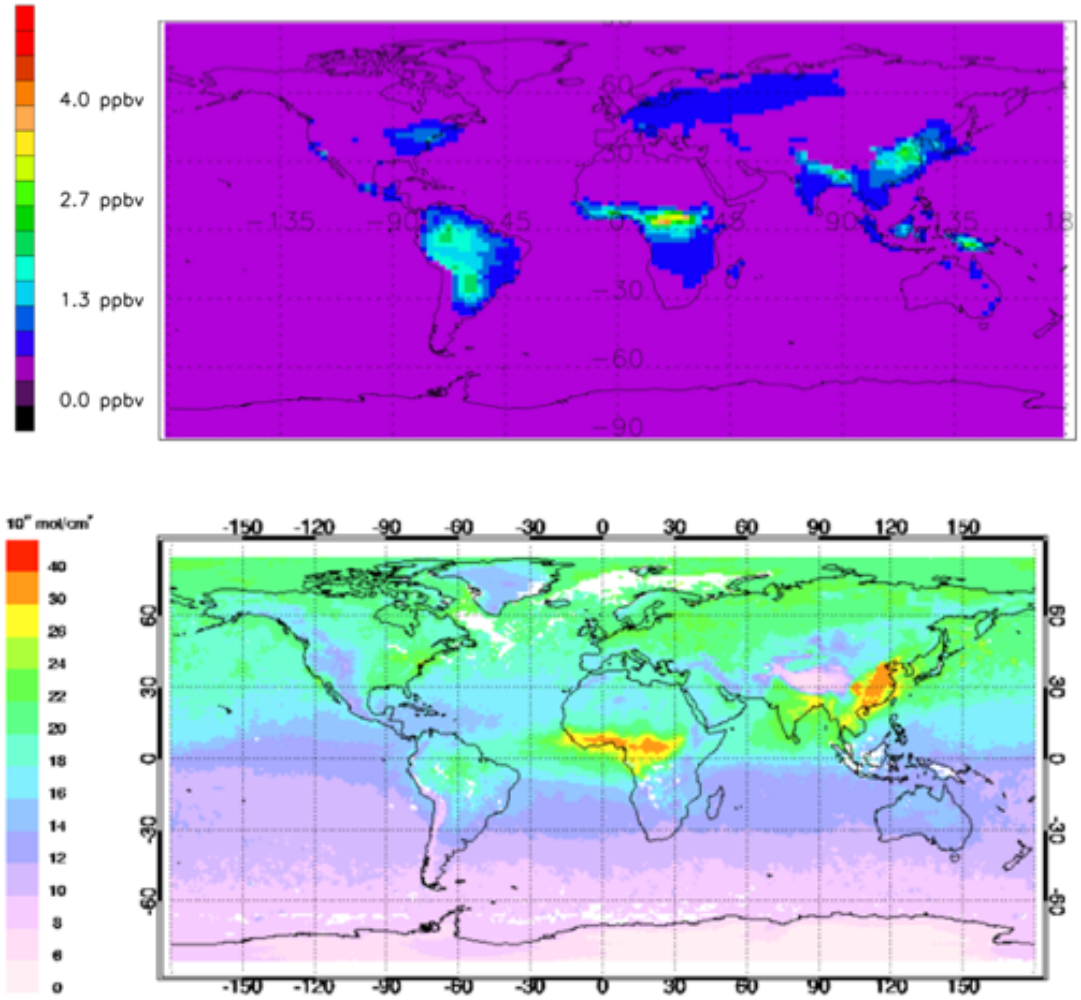

Figure. 11 (a) GEOS-Chem model estimated global average emissions of C_2H_4 primarily in the Sub-Saharan Africa region (0˚ and 45˚ lon and 0˚and 14˚lat) in the month of December 2009. This indicates all volume mixing ratios greater than 700 mbar, the highest being over 2.7 ppbv, indicates a relatively high C_2H_4 period. (b) MOPPITT map showing lowest elevated levels of CO in 2013 for month of December, indicating possible source for C_2H_4 from non-biogenic lofting processes according to the profile generated from GEOS-Chem model.
(Source: https://www.acom.ucar.edu/mopitt/MOPITT/data/plots/maps.html)

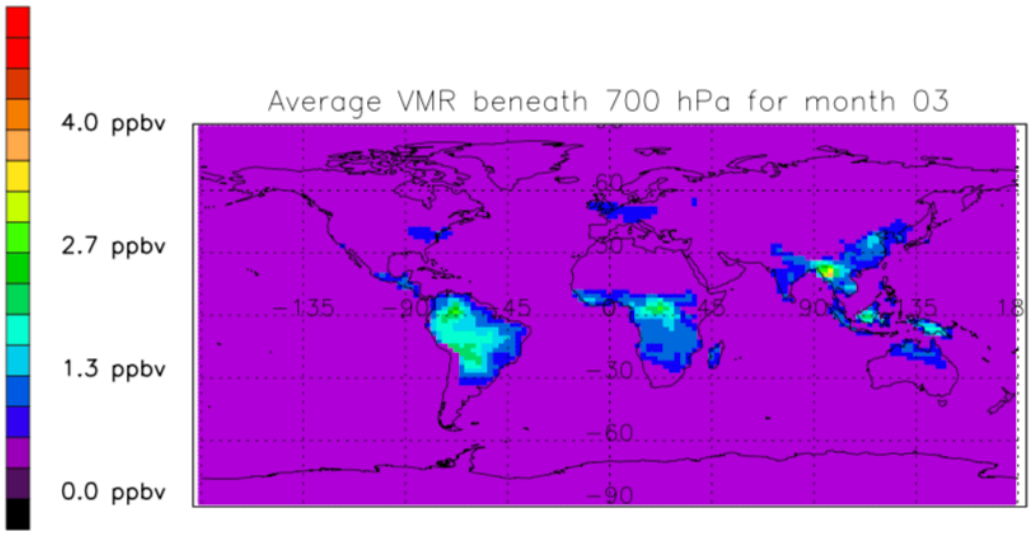

(a)

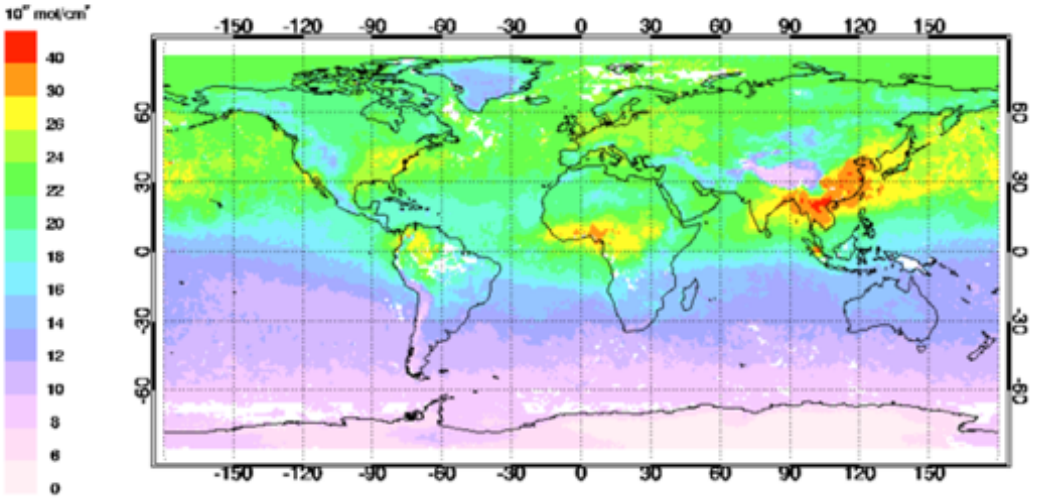

(b)

Figure 12. (a) GEOS-Chem model indicating highest estimated global average emissions in ppbv of C_2H_4 primarily in the South Asian regions (92° and 112° lon and 16° and 30° lat) in March of 2009. Map shows VMR greater 700 mbar, the highest being over 4.0 ppbv. (b) MOPPITT map showing highest elevated levels of CO in 2013 for month of March, indicating a co-location between the same time periods of global CO and C_2H_4 emissions.
(Source: https://www.acom.ucar.edu/mopitt/MOPITT/data/plots/maps.html)

CHAPTER 4

Results

4.1 Selection of Interesting Regions/Months

From the previous chapter we narrowed our selection of prime C_2H_4 emitting regions to three locales along the equator. We chose the Sub-Saharan African region at coordinates 0° and 45° lon and 0°and 14°lat, Amazonian region at -70°and -55° lon and -28° and 4°lat and South Asian region at 92° and 112° lon and 16° and 30° lat. These areas simulated from the GEOS-Chem model, show the highest average near-surface VMR of C_2H_4. The Amazonian region showed elevated C_2H_4 VMR values at near 2.7 ppbv from possible biogenic sources in the month of May in 2009. To further enhance this view, we compared MOPPITT CO maps for the same coordinates displaying lower CO emissions for the month of May. CO emissions typically coincide with biomass burnings. For surface observations we need to compare both instruments in observation quality or number of data points collected to verify C_2H_4 signal from the surface. This is vital due to instrument noise and difficulty in detecting elevated C_2H_4 close to the surface.

4.2 Number of Observations in Chosen Regions for both TES & CrIS Instruments

Within the regions chosen, TES and CrIS differ in size of spatial sampling. CrIS is less fine in spectral resolution than TES, but has higher spatial coverage (Shephard et al., 2015). Three criteria are usually traded off when considering measurements from an infrared remote sounding instrument:

1. Spectral resolution, which controls what specific features are measured within a spectrum or measuring the composition of medium
2. Spatial resolution, which determines level of detail that is observed for the target

3. Signal-to-noise (S/N) which determines the amount of desired signal of target versus instrument noise or background noise

These three factors help in determining the number of observations needed in order to detect a significant signal strength to that of the instrument noise. We compare the signal strength to that of the instrument noise generated by both instruments in order to determine the number of measured footprints needed to be able to detect C_2H_4 signal. The satellite foot print of CrIS is 2200 km wide swath, yet has a lower spectral resolution of 0.625 cm^{-1}. The TES instrument consists of lower spatial resolution of 5 km x 8 km wide swath, yet a higher spectral resolution of 0.06 cm^{-1}. A more localized observation would be in order for C_2H_4 via TES. In order to obtain a strong signal-to-noise for C_2H_4 from surface we need a large number of observations or data points within the coordinates selected. Figure 13 shows the difference between TES and CrIS observation data points. The TES swath is standard for one month's worth of data, while the observation points shown on the CrIS figure is for one day's worth. In the CrIS figure we see a much more densely populated number of nadir data points in one day's rather versus one month's worth of TES data. CrIS can generate more data points allowing for a lower detection threshold for high concentrations of C_2H_4. These data points are then converted to spectral radiance measurements through the radiative transfer algorithm. The actual signal strength is observed though a brightness temperature difference spectra.

4.3 Simulated Brightness Temperature Differences One or Multiple Profiles (TES vs. CrIS)

Data from spatial sampling are measurements of radiance from the Earth (both sampled through absorption and extinction), which are measured in W/cm^2 sr cm^{-1}. This radiance spectra are processed via radiative transfer model within the instruments data retrieval methods. They are then converted to brightness-temperature spectra, which shows the signal strength of the species of interest. We calculate the spectrum with zero C_2H_4 in the atmosphere, then calculate the spectrum with a non-zero C_2H_4 profile, then take the difference to see the magnitude of the C_2H_4 signal. This difference is measured with respect to a reference wavelength window channel, that does not contain the C_2H_4 species. We evaluated the magnitude of the expected brightness temperature signal for a C_2H_4 profile which we generated via the GEOS-Chem model over the Amazonian region (see figure 8). Other input variables, such as temperature profile, were also used from the TES and CrIS retrievals (see chapter 3.2). Figures 14 and 15 show simulated brightness temperature spectra for C_2H_4. They cover an atmospheric window between 940 and 960 cm^{-1}. The feature shows a BTD of 0.05 K near the 950 cm^{-1} (also consistent with previous studies discussed in chapter 2) wavelength for both CrIS and TES instruments at a thermal contrast of 0 K. Dolan et al. (2016) showed that a high thermal contrast would be needed to order to minimize VMR needed to detect a significant signal strength. A higher signal can be achieved if there is a larger thermal contrast between the surface and some altitude immediately above the surface. BTD plots can change depending on thermal contrast, as well as with the C_2H_4 profile, temperature profile, surface temperature, water vapor profile and emissivity. All information used in such plots was from TES and CrIS

retrievals products. Other areas chosen as the African or Asia region have different profiles of C_2H_4 that can affect the signal strength. The VMR values in the vertical range can fluctuate over decreasing pressure range shown in figure 8(b). There can be a significant increase in the VMR throughout increasing altitude indicating a lofting process. This lofting can signify a non-biogenic source. Emissions of C_2H_4 from the biogenic surface sources would exhibit a steady increasing profile, indicating a steady average of C_2H_4 VMR being emitted from the surface. Lofting processes would disrupt such a profile (see figure 8(b)).

Figures 14 and 15 also show a dashed line indicating the single-footprint noise level for both the TES and CrIS instruments. For TES the instrument noise is 0.15K and 0.04K for CrIS. The instrument noise for TES is higher indicating that more observation footprints are needed to detect C_2H_4. This is a S/N factor of 1/3. We would require $\sqrt{(\#\ of\ Obs.\ avg.)} = 3$ in order to generate a S/N factor of 1. This is equal to 9 TES footprint observations. For the CrIS the S/N is 1, indicating that the C_2H_4 signal from this input profile could be detected in a single CrIS footprint Having such a thermal contrast is key in being able to detect surface C_2H_4 signal. This is done by getting a higher spatial average.

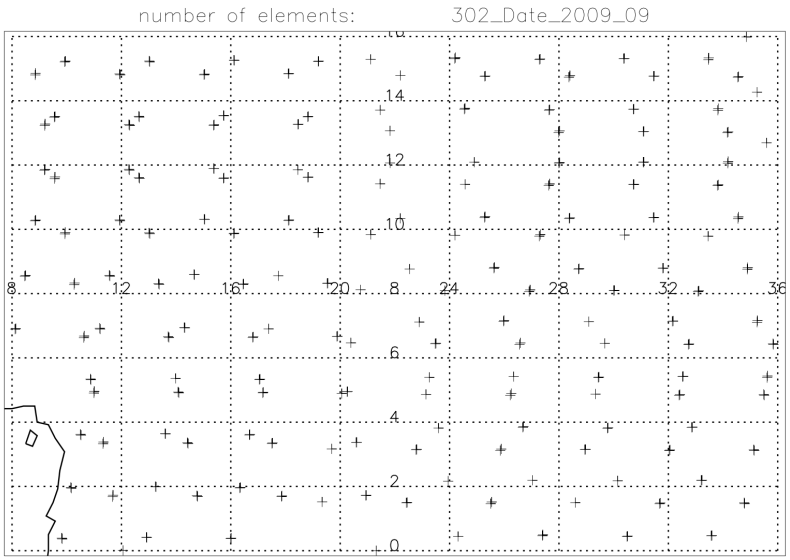

(a)

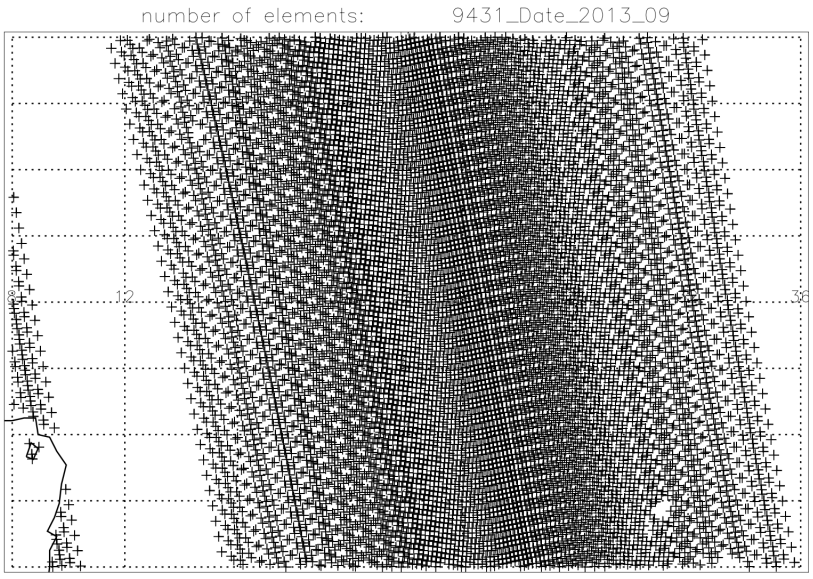

(b)

Figure 13. (a) TES spatial sample grid for Amazon coordinates indicating only 302 data points collected during a TES scan for the full month of September (b) indicates CrIS spatial sample grid showing 9431 data points collected on one day time scan during a, indicating a significant increase in spatial coverage for coordinates located in Amazon region.

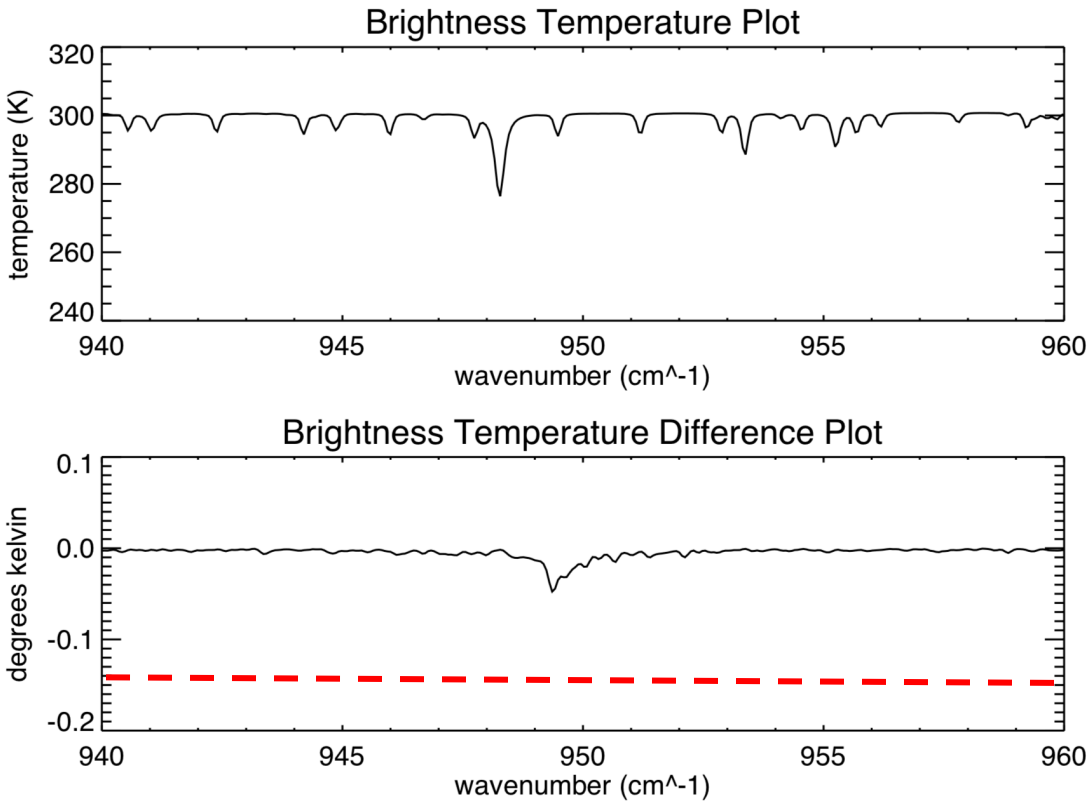

Figure 14. TES simulated brightness temperature difference plot. Shows a spectral atmospheric window range from 940 to 950 cm^{-1} with the C_2H_4 signal shown near the 950 cm^{-1} wavelengths. The red dashed line shows the TES instrument noise at 0.15K. The noise is 3 times higher than the C_2H_4 signal, indicating that at least 9 footprints are needed to equal a S/N of 1.

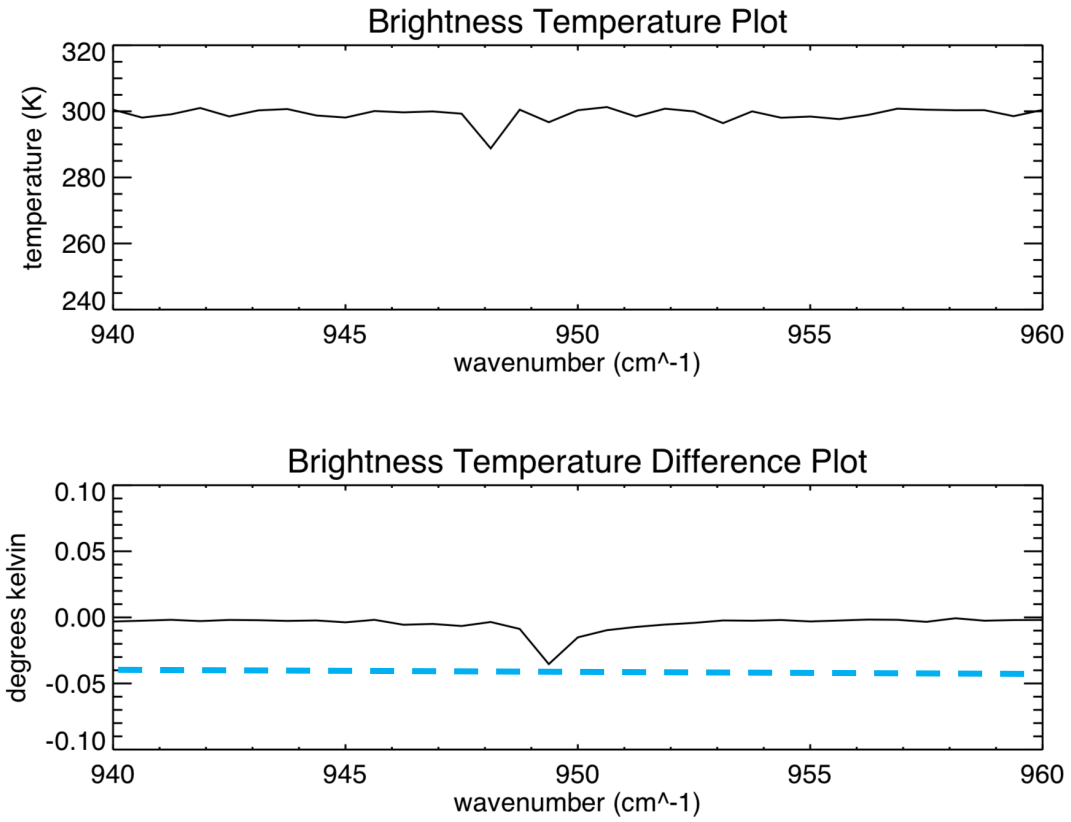

Figure 15. CrIS simulated brightness temperature difference plot. Shows a spectral atmospheric window range from 940 to 950 cm^{-1} with the C_2H_4 signal shown near the 950 cm^{-1} wavelengths. The blue-dashed line shows CrIS thermal noise equal to 0.04K. This is S/N ratio of 1, indicating a single footprint of observation is needed to detect C_2H_4 signal.

CHAPTER 5

Discussion

From the results of our BTD plots, we can assess future plans for biogenic surface C_2H_4 detection via the CrIS instrument, if current models and simulations are true. We have constructed a case showing from previous studies and current global models that detection limits of surface biogenic C_2H_4 VMR is possible given the current VMR amounts at the given locations and times of the year. These areas were located in the Amazon region, Sub-Saharan Africa and southern Asia. Model profiles generated from current GEOS-chemistry transport model showed steady increasing VMR from two areas of Asia and South America. The African region showed a possible lofting mechanism from a likely biomass burning. We can assure at least two location for future study of satellite detection of C_2H_4 VMR. We further isolated possible lofted biomass burnings by showing CO maps from MOPPITT indicating increased CO in the atmosphere. CO and C_2H_4 VMR co-location indicate usual biomass burnings. We also showed a map indicating no CO emissions, with relatively high C_2H_4 VMR at around 2.7 ppbv in the Amazon region, indicating non-fire plume lofted C_2H_4 sources. The profiles generated for this region indicate a near smooth flux of C_2H_4 VMR, which also contributes to a possible biogenic non-lofting source. BTD plots have shown instrument capability to reach detections of elevated C_2H_4 VMR near the surface, given that the instrument noise is low enough, that enough radiance measurements are collected (given a high thermal contrast) and averaged. CrIS is capable of a single footprint of observation to achieving this threshold detection.

For potential future observation we need to further distinguish between lofted biomass burnings and natural surface biogenic emissions. This can be done with in-situ aircraft campaigns compared to spaceborne satellite detection. We can also run our model for a larger variety of time periods and thermal contrasts to further distinguish a pattern of biogenic sources of C_2H_4. We can further generate different model profiles from GEOS-Chem within that larger variety timeframes and help distinguish between lofted or non-lofted C_2H_4 sources.

In all, we have the current capability to determine C_2H_4 detection under circumstances that generate fire-plumes. Non-fire plume biogenic sources can help in quantifying contributions of ethylene to the troposphere and help further understand it's impacts on the ozone, global warming, and human health.

REFERENCES

[Aiken et al., 1982] A.C. Aikin, J.R. Herman, E.J. Maier, C.J. McQuillan (1982). Atmospheric Chemistry of Ethane and Ethylene Journal of Geophysical Research, vol. 87, no. c4, pages 3105-311

[Alvarado et al., 2011] Matthew J. Alvarado, Karen E. Cady-Pereira, Yaping Xiao, Dylan B. Millet and Vivienne H. Payne (2011). Emission Ratios for Ammonia and Formic Acid and Observations of Peroxy Acetyl Nitrate (PAN) and Ethylene in Biomass Burning Smoke as Seen by the Tropospheric Emission Spectrometer (TES)Atmosphere, 2, 633-654

[Beer, R., et al., 2001] Tropospheric emission spectrometer for the earth observing System's Aura satellite. Appl. Opt. 44, 2356-2367

[Bey et al., 2001] Isabelle Bey, Daniel J. Jacob, Robert, M. Yantosca, Jennifer A. Logan, Brendan D. Field, Arlene M. Fiore, Qinbin Li, Honguy Y. Liu, Loretta J. Mickley, and Martin G. Shultz (2001). Global Modeling of Tropospheric Chemistry with Assimilated Meteorology: Model Description and Evaluation, Journal of Geophysical Research, Vol. 106, No. D19, Pages 23, 073-23, 095

[Chuong and Stevens 2000] Chuong, B and Stevens, P.S., (2000). Kinetic Study of the OH + Isoprene and OH + Ethylene Reactions between 2 and 6 Torr and over the Temperature Range 300-423 K, Journal Physical Chemistry A 2000, 104, 5230-5237

[Dolan et al., 2016] Dolan, W., Payne, V.H., Kualwik, S.S., Bowman, W.S., (2016). Satellite observations of ethylene (C 2H 4) from the Aura Tropospheric Emission Spectrometer: A scoping study, Atmospheric Environment, 14, 388-393

[Drummond, J. R., and G. S. Mand, 1996] Drummond, J. R., and G. S. Mand (1996). The Measurements of Pollution in the Troposphere (MOPITT) Instrument: Overall Performance and Calibration Requirements, Journal of Atmospheric and Oceanic Technology, *13*(2), 314–320

[Folberth et al., 2006] G. A. Folberth, D. A. Hauglustaine, J. Lathi`ere, and F. Brocheton (2006). Interactive chemistry in the Laboratoire de M´et´eorologie Dynamique general circulation model: model description and impact analysis of biogenic hydrocarbons on tropospheric chemistry, Atmos. Chem. Phys., 6, 2273–2319

[Hauglustaine et al., 1994] Hauglustaine, D. A., Hourdin, F., Jourdain, L., Filiberti, M. A.,Walters, S., Lamarque, J. F., and Holland, E. A., (1994) Interactive chemistry in the Laboratoire de Meteorologie Dynamique general circulation model: Description and background tropospheric chemistry evaluation, J. Geophys. Res., 109

[Lacis et al., 1990] Andrew Lacis and Donald J. Wuebbles (1990). Radiative Forcing of Climate by Changes in the Vertical Distribution of Ozone, Journal of Geophysical Research, vol. 95, No. d7, 9971-9981L

[Li et al., 2006] Wenhong Li, Rong Fu and Robert E. Dickinson (2006). Rainfall and its seasonality over the Amazon in the 21st century as assessed by the coupled models for the IPCC AR4 Journal of Geophysical Research, vol. 111, d02111, doi:10.1029/2005JD006355

[Payne et al., 2014] V. H. Payne, M. J. Alvarado, K. E. Cady-Pereira, J. R. Worden, S. S. Kulawik, and E. V. Fischer., (2014). Satellite observations of peroxyacetyl nitrate from the Aura Tropospheric Emission SpectrometerAtmos. Meas. Tech., 7, 3737–3749, doi:10.5194/amt-7-3737-2014

[Rudolph et al., 1989] Rudolph, J., Khedim, A, Wagenbach, D., (1989) The Seasonal Variation of Light Nonmethane Hydrocarbons in the Antarctic Troposphere, Journal of Geophysical Research, vol. 94, D10, 13039-13044

[Sawada et al. ,1986] Shinichi Sawada and Tsumugu Totsuka (1986). Natural and Anthropogenic Sources and Fate of Atmospheric Ethylene, Atmospheric Environmental Vol. 20, No. 5, pp. 821 -832

[Shephard et al., 2015] M.W. Shephard and K.E. Cady-Pereira (2015). Cross-track Infrared Sounder (CrIS) satellite observations of tropospheric ammonia, Atmos. Meas. Tech., 8, 1323–1336, doi:10.5194/amt-8-1323-2015